A PHOTOELASTIC ANALYSIS OF A BEAM WITH A LARGE SYMMETRICALLY LOCATED HOLE

by

Donald John Duffy

Thesis submitted to the Graduate Faculty of the

Virginia Polytechnic Institute

in candidacy for the degree of

MASTER OF SCIENCE

in

Applied Mechanics

APPROVED:

Director of Graduate Studies

APPROVED:

Head of Department

Dean of Engineering

Major Professor

February, 1958

Blacksburg, Virginia

I. TABLE OF CONTENTS

		Page No.
II.	List of Figures	3
III.	Notation	4
IV.	Introduction	5
V.	Review of Literature	6
VI.	The Investigation	7
	A. Object of the Investigation	7
	B. The Apparatus and Model	7
	C. Testing Procedure	10
	1. Preparation of the Model	10
	2. Testing Program	16
VII.	Discussion of the Results	17
VIII.	Conclusions	21
IX.	Appendix	22
	A. The Shear Difference Method applied across Upper Section O-L as shown in Figure VI-a	22
	B. Resulting stress distributions (σy) across Lower Sections O-L, O-M, and O-R and across Upper Sections O-M, O-L, and O-R	34
	C. Effects of friction forces	37
X.	Acknowledgement	40
XI.	Bibliography	41
XII.	Vita	42

II. LIST OF FIGURES

Figure No.	Title	Page No.
I.	Elements of the Polariscope.....	8
II.	Loading Scheme.....	9
III - IV.	Calibration Curves.....	11 - 12
V.	Edge Stresses.....	15
VI. a,b,c	Fringe Patterns & Dimensioned Specimen...	19
VII.	Superimposed Isoclinics.....	20
VIII - IX.	θ vs X, O-L, I-L, II-L,- Isoclinic Parameter vs. Position Upper Portion.....	23 - 24
X - XII.	p-q vs X, O-L, I-L, II-L,- Upper Portion.	25 - 27
XIII.	$\Delta\gamma_{xy}$ vs X, O-L Upper Portion.....	29
XIV.	γ_{xy} vs X, O-L Upper Portion.....	30
XV.	σ_x vs X, O-L Upper Portion.....	32
XVI.	σ_y vs X, O-L, O-R Upper Portion.....	33
XVII.	σ_y vs X, O-L, O-R, O-H Lower Portion.....	35
XVIII.	σ_y vs X, O-H Upper Portion.....	36

III. NOTATION

SYMBOL		DEFINITION
σ_x, σ_y	.....	Normal stress components parallel to X and Y axes.
τ_{xy}	.....	Shearing stress component in rectangular coordinates.
X, Y	.....	Rectangular components of a distributed surface force per unit area.
p	.....	Maximum principal stress.
q	.....	Minimum principal stress.
θ	.....	Isoclinic parameter.
n	.....	Fringe order.
f	.....	Material fringe constant. #/fringe/in.
P	.....	Load applied to specimen in pounds.
F	.....	Model fringe value psi/fringe.

IV. INTRODUCTION

Many instances arise in the assembly or operations of structural or mechanical parts which require that holes be cut in beam members of the assembly. For a proper design, knowledge of the stresses existing within the interior regions as well as on the boundaries of the beam is required.

The state of stress developed in a beam of constant cross sectional area, subjected to pure bending is considered as a plane stress problem. Due to the complicated boundary conditions arising from the holes, a rigorous mathematical solution for the plane stress problem is rather difficult, though not altogether impossible. However, certain experimental methods together with some numerical approximations for solving the equilibrium and boundary condition equations have been developed which enables one to handle the problem with sufficient accuracy for engineering purposes. (1)*

It should be remembered that in using the method of photoelasticity, difficulties in the techniques are encountered, namely:

a. Maintaining of symmetry of specimen and load;

b. Minimizing edge stresses; and

c. Minimization of friction forces under load and reaction points.

Consequently, a major portion of this thesis will be devoted to a consideration of the experimental difficulties and the techniques developed for overcoming them.

---

* Numbers in parenthesis refer to reference in Bibliography.

V. THE REVIEW OF LITERATURE

The discovery of the photoelastic effect in 1816 is attributed to Sir David Brewster (2). However, it was not until 1900 that its application was recognized.

Since 1900, there has been considerable work published on the flexure of beams. In 1927, Maris (3) investigated the stress distribution in notched beams subjected to uniform bending moments. During this same year, Coker worked on the effects of varying beam depths and span lengths on the stress distribution. He also investigated notched beams subjected to a uniform bending stress in 1930. In 1934, Wahl and Beeuwkes employed the photoelastic techniques to determine the stress distribution in notches and fillets subjected to a uniaxial state of stress (4). They also have tabulated values for stress concentration factors. Frocht (5), in 1935, tabulated values in addition to those given by Wahl and Beeuwkes, for notches and fillets subjected to a uniform or constant bending moment.

In more recent times, Hartman and Leven (6), in 1950, have compiled factors of stress concentration for fillets in a field of pure bending.

VI. THE INVESTIGATION

A. Object of the Investigation:

The objectives of the investigation were:

a. To develop techniques for minimizing experimental difficulties, and

b. To determine the stress distribution across arbitrary sections by using the Shear Difference Method.

B. The Apparatus and Model:

1. The experimental work for this investigation was conducted in the Photoelasticity Laboratory of the Applied Mechanics Department, at Virginia Polytechnic Institute. The apparatus consisted mainly of a standard portable General Radio diffuser polariscope, type number 153hA, a Chapman loading frame, type number 482, and a Graphlex camera mounted on a lathe bed. The setup of the apparatus is illustrated in FIGURE I.

a. The diffuser type polariscope is used to convert a beam of natural or unpolarized light into plane or circularly polarized light depending on whether a standard or crossed plane polariscope is desired. The source of light used for the polariscope was a strobolume type 1532-a, manufactured by General Radio. The duration of light from this source is 30-40 micro-seconds.

b. The loading frame: The method of loading by use of the loading frame is demonstrated in FIGURE II. This frame makes use of a linear spring which has been previously calibrated. The spring is attached to a dail mechanism which measures the deflection in thousandths of an inch. The calibration factor is 1.3#/0.001 inches of deflection.

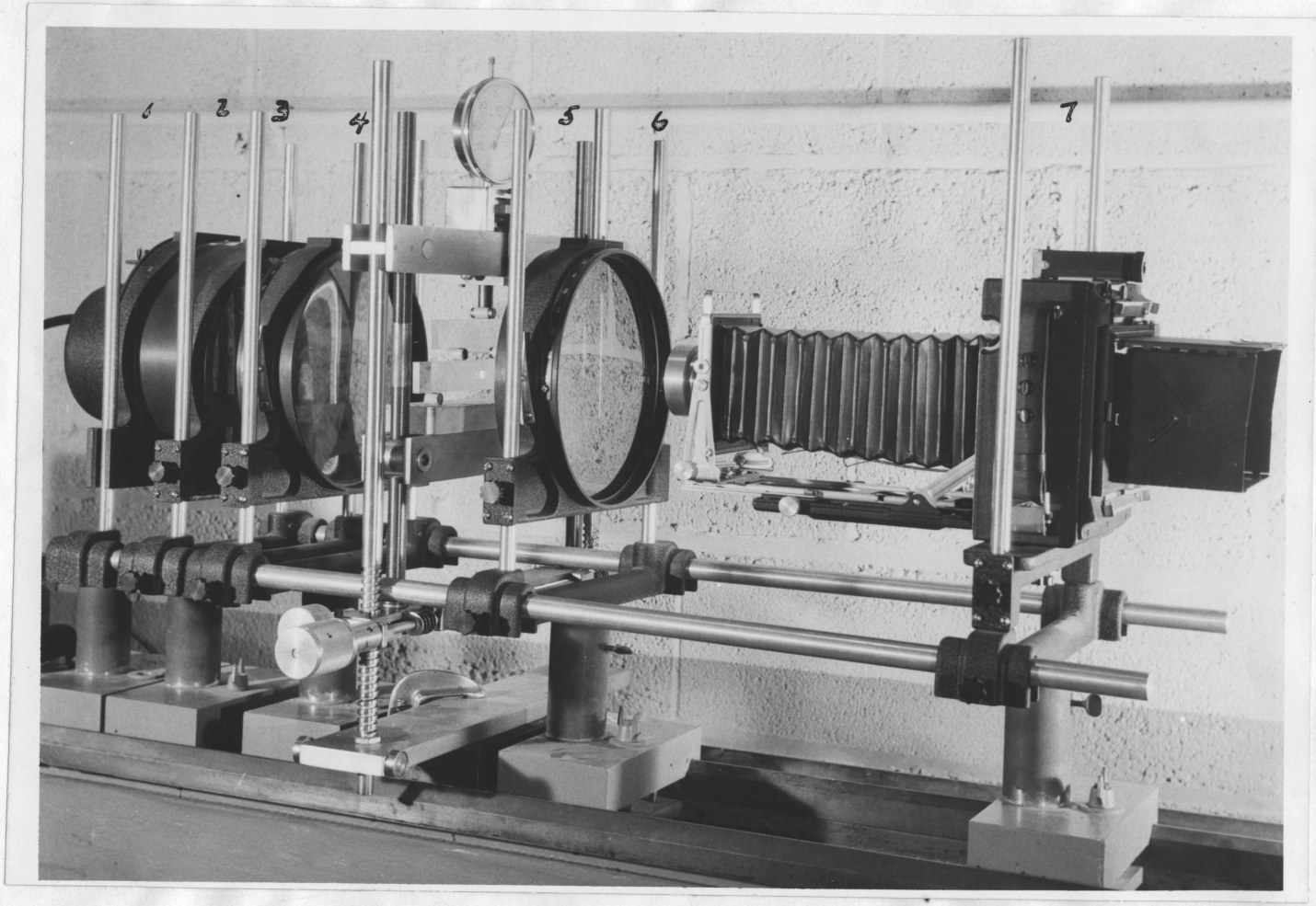

Figure I. Elements of Polariscope

(1) Strobulume (2) Lens (3) Filter (4) Polarizer and Quarter Wave Plate (5) Photoelastic Model and Loading Frame (6) Analyzer and Quarter Wave Plate (7) Camera

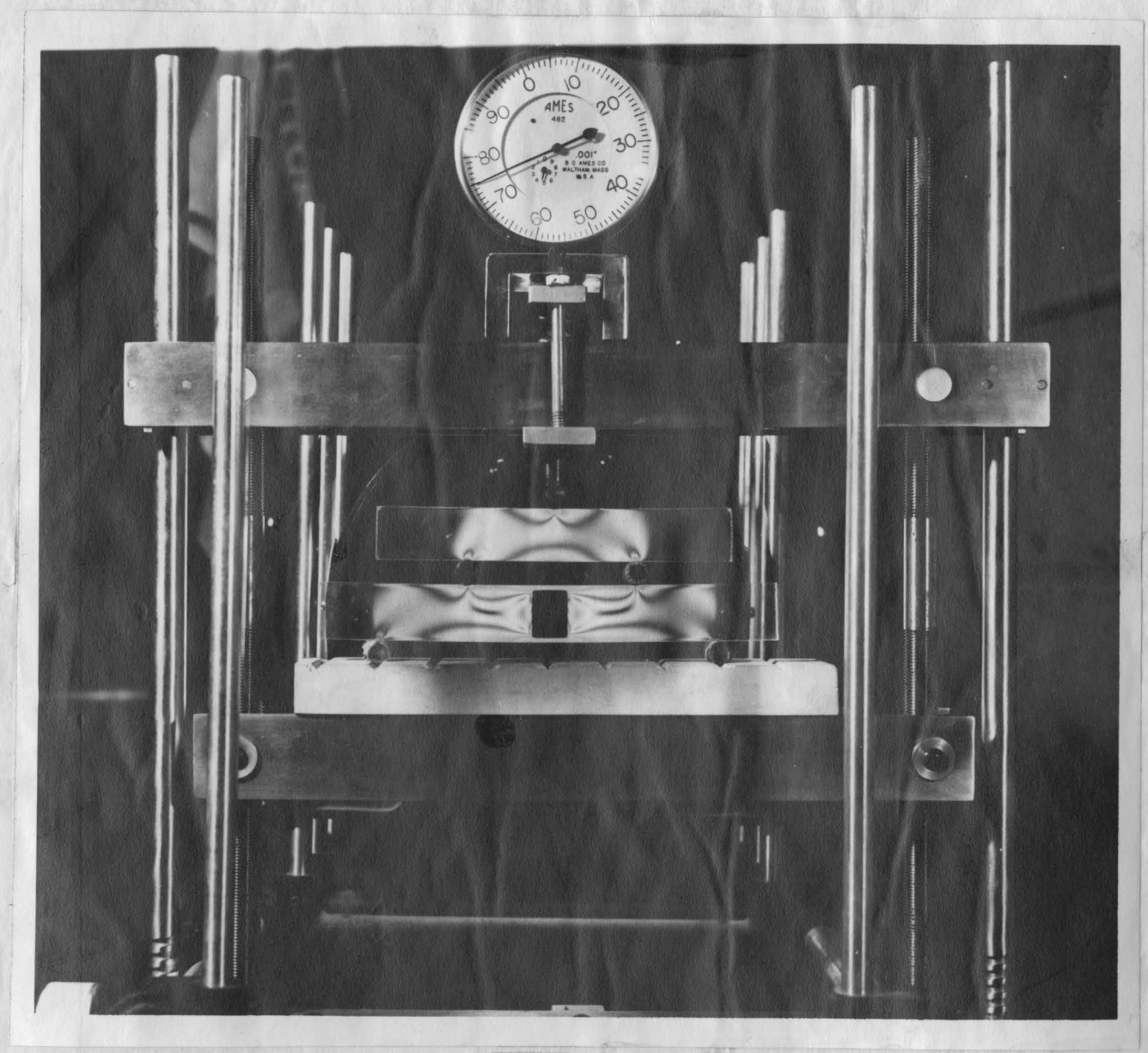

Figure II. Loading Scheme

Note that the loads are outside the hole in the above photograph. See also Figure VI-c. The positioning of the loads for the problem investigated is shown in Figures VI-a and VI-b.

2. The model material used for this investigation was CR-39. For determining the material fringe constant, the calibration was performed with a bending and a tensile specimen. A sketch of the specimens is shown below; calibration test data are presented in FIGURES III and IV.

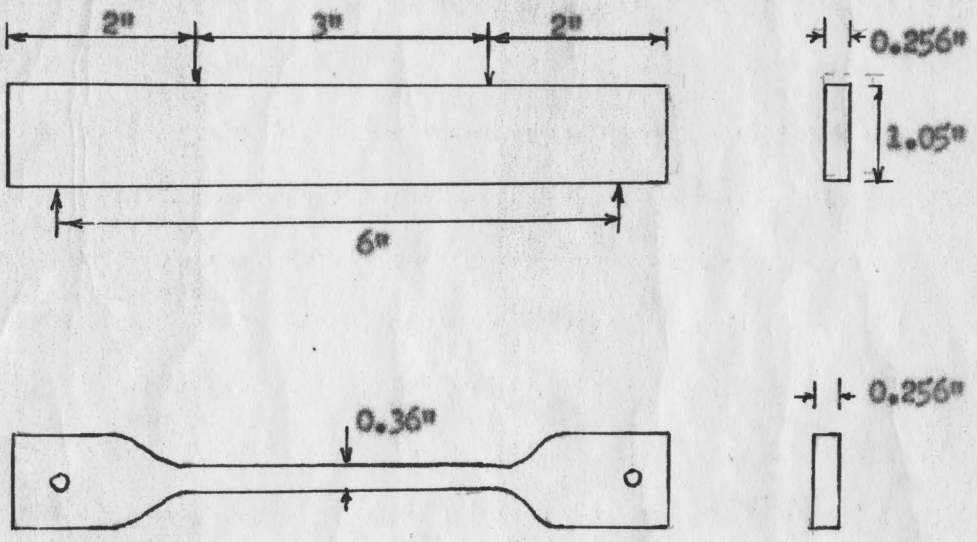

C. Testing Procedure:

1. Preparation of the Models:

The model was made by the use of a Chapman photoelastic model making kit. In using this kit, the model material plate was first cut to within one-half inch of the final dimensions by using a high speed short stroke jig saw. Next, using a master template, prepared out of 0.100" sheet aluminum, the rough model was fixed to the template by utilizing special jigging tape. The template, when fixed to the rough model, guides the plastic against the cutter to within 0.007" of the finish line using the rough plug of the high speed spindle. A finishing plug is then inserted and the model is brought to the final dimensions of the template.

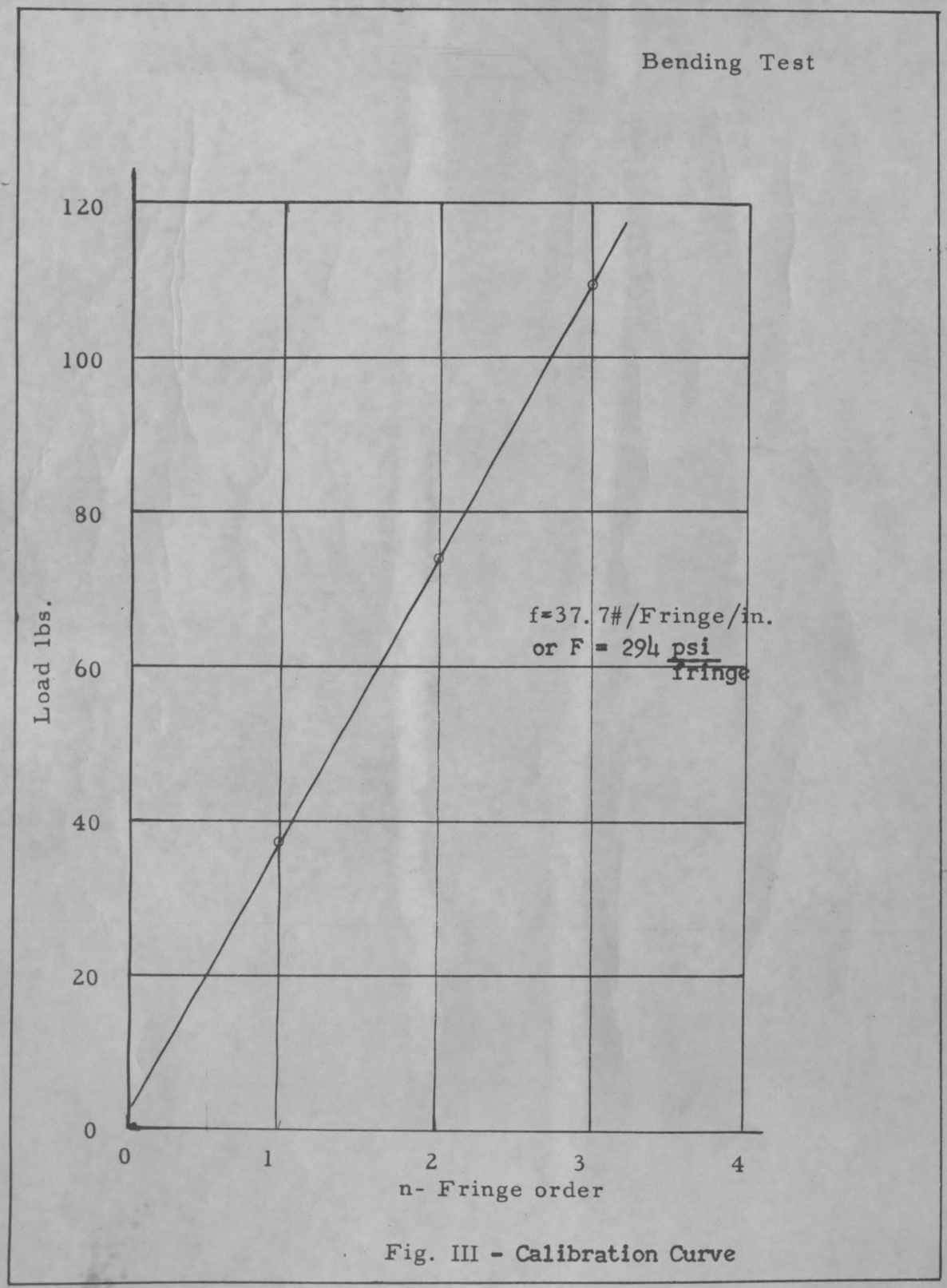

Fig. III - Calibration Curve

Tension Test

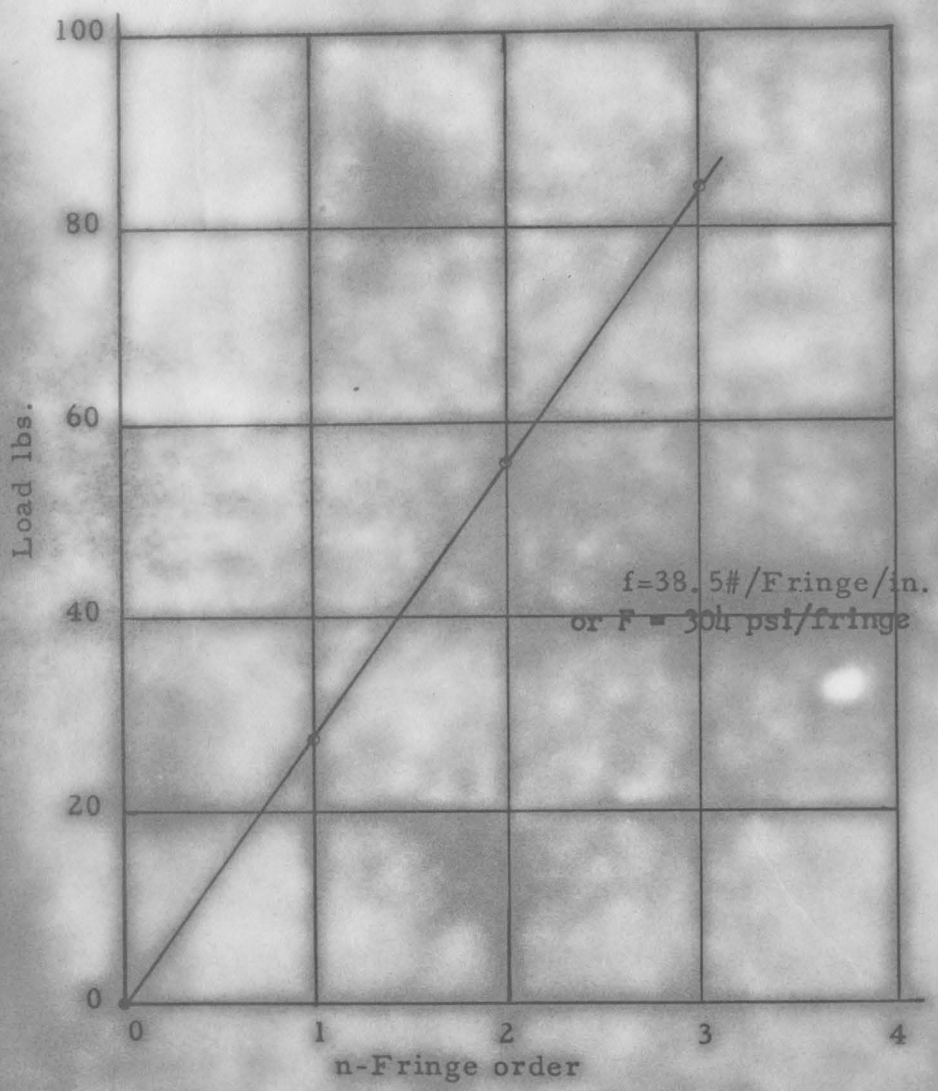

Fig. IV - Calibration Curve

In making the holes, first, a quarter-inch round hole was made by means of an ordinary bench drill. Next, using a double steel template, which was cut to the required dimensions of the hole, the model was inserted between it and the composite assembled in a vise. Finally, the required dimensions of the hole were achieved by hand filing.

As a precaution against the formation of edge stresses, the following techniques were used.

a. In cutting, fast sweeping feeds and small depths of cuts were used.

b. In drilling, the operation was performed with the model submerged in water.

c. In filing, the file used was frequently changed.

The above techniques were employed for the purpose of reducing the edge stresses developed through machining. After some experiments, the machining stresses were virtually eliminated by using the pro - cedure outlined above. This achievement is considered especially important since it was accomplished without employing an annealing process which is sometimes used to reduce these stresses. Also, annealing the material often detrimentally warps the model upon the release of machining stresses.

All plastics contain moisture, some of which is free and some of which may be in chemical combination with the material. After machining, an exposed layer of new material is left along the machined edges. If the moisture content of this newly exposed material is in a state of equilibrium with the moisture in the air, no edge stresses developed

by the time-edge effect will result. If not, the condition is unstable and then, in one case, the new edge material may procure moisture from the air, thus causing the material to expand and develop compressive edge stresses. On the other hand, the material may lose moisture to the air causing the material to shrink and develop tensile edge stresses. Trial models used in this investigation began to develop edge stresses within three hours after machining. At first, the models were stored in a dessicator containing sulphuric acid, but this was considered generally unsatisfactory. A better method of storage, though still not providing complete protection, was accomplished by storage in halowax oil. For the experiments discussed, the latter method of storage is considered as the better method. In the present investigation, however, all tests were run on halowax oil coated specimens within two hours of final machining operation, thus virtually eliminating the time-edge effect in these tests. The effectiveness of the halowax oil in minimizing edge stresses is shown in FIGURE V. Since the model was free of all residual stresses in a short time after unloading, the lower photograph shows the edge stresses developed in halowax oil.

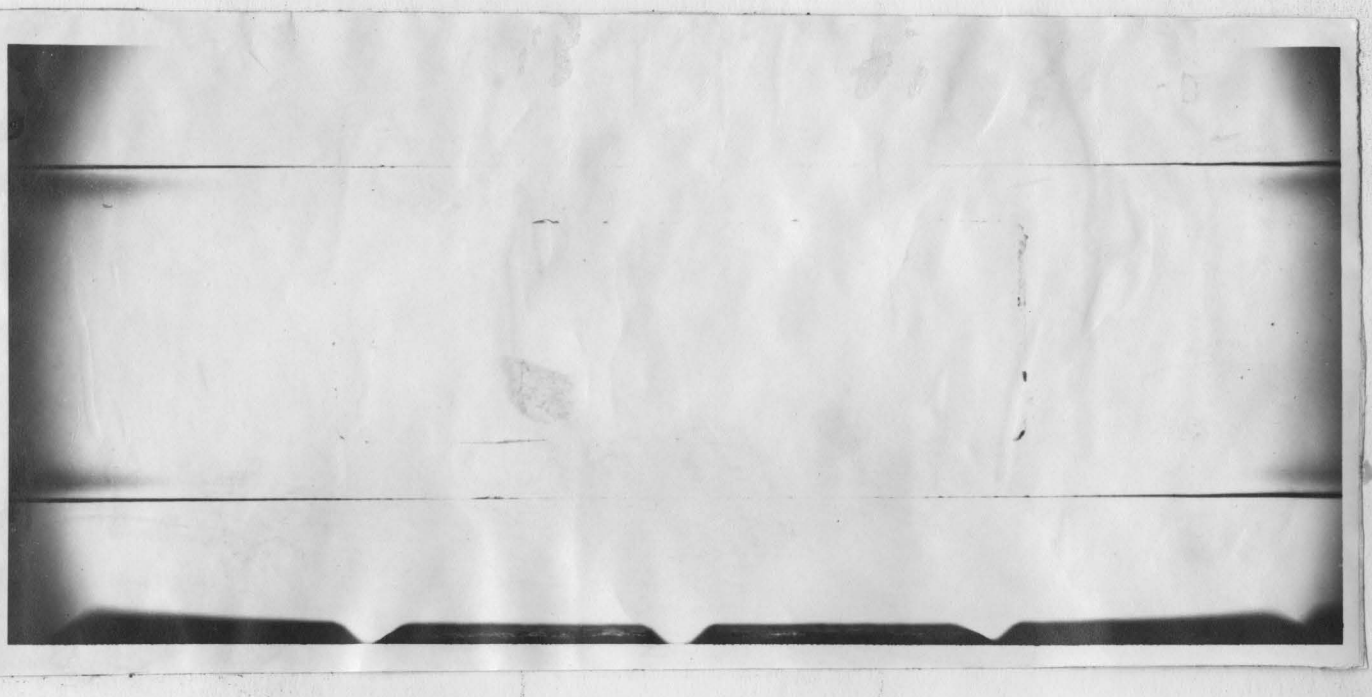

Before Loading

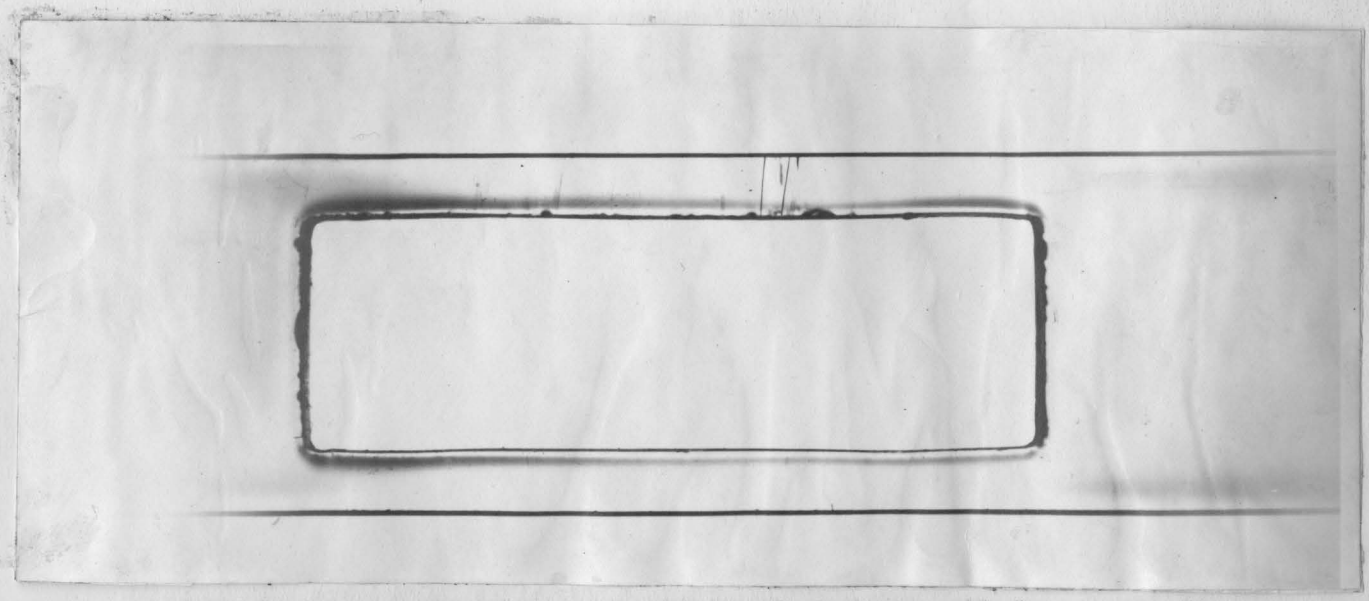

After loading, unloading, and storing in Halowax Oil for one week.

Figure V. Edge Stresses

2. Testing Program:

Before starting the test, all the components and accessories of the polariscope were properly aligned along a common axis; both vertical and horizontal alignment were checked. The camera for photographing the various patterns was located so that a sharp edge image appeared over the ground glass. With all the elements properly aligned the clamp screws which fastened the accessories to the lathe bed were tightened.

Next, the model was supported on small pieces of three-eighths inch diameter rods so as to approach the conditions of a simple support. The bending moment was transmitted to the model as shown in FIGURE II.

The isoclinics were photographed in this investigation. In obtaining the isoclinics only a very small load was applied, since the isoclinic parameters are independent of the load and if a larger load had been used, additional lines would have appeared corresponding to the ischromatics. The parameters photographed were the 15°, 30°, 45°, 60°, 75°, and 90° isoclinics. In order to increase the distinctness of the isoclinics, a white light source was used instead of a monochromatic source. Also, an F-16 lens opening and two flashes from the strobulume were required for sharp pictures.

For the fringe patterns, the maximum permissible load was used since this produced the sharpest pictures. These patterns photographed best using an F-8 lens opening and sixteen flashes of the strobulume lamp.

VII. DISCUSSION OF RESULTS

From the data obtained, namely the fringe patterns and the isoclinics, coupled with the boundary conditions, the stress distributions have been determined by the Shear Difference Method. The boundary conditions used in all cases have been that the stresses existing on the boundaries of the beam as well as around the boundaries of the hole are zero. That is:

$$\tau_{\text{tangent to boundary}} = 0$$

$$\sigma_{\text{normal to boundary}} = 0$$

The dimensions, load points, and sections analyzed for the problem investigated are presented in FIGURE VI (a).

The fringe pattern for the problem considered is shown in FIGURE VI(b), and a schematic representation of the isoclinics in the region of the upper section O-L is shown in FIGURE VII. Also shown is a fringe pattern in FIGURE VI(c) for the case where the load points are beyond the lateral limits of the hole. This fringe pattern is included only to point out the differences developed by altering the position of load points. The isoclinic pattern for the model pictured in FIGURE VI(c) above and below the hole consisted of only one parameter; this being the zero isoclinic parameter. Therefore, the stress distribution through the center of this beam may be obtained directly from the fringe pattern. However, this pattern is only presented for comparison purposes and the stress distribution will not be included.

Examination of the fringe pattern presented in FIGURE VI(b) indicates dissymmetry of loading. In order to obtain the effect of this

dissymmetry on the stress distribution, sections were analyzed at symmetrical locations on either side of the beam's center line. The sections analyzed were designated O-L, O-M, and O-R, and the locations of these sections are shown in FIGURE VI(a). The data, curves and tables required for the Shear Difference Method applied across upper section O-L are reported in Appendix A. The calculations required for section O-R are similar to those for section O-L, and will not be included. As seen from FIGURE XVI, the results show that the effect of the dissymmetry upon the stress distributions (σ_Y) is small. The important thing to note in examining the normal stress (σy) distribution for upper sections O-L and O-M of the beam is that there is a reversal of curvature encountered near corners of the hole.

A photoelastic analysis in FIGURE VI(b) of sections O-L, O-M and O-R below the hole showed that only the zero isoclinic parameter was present throughout these sections. Therefore, the shearing stress was zero at each station across these sections. This is similar to the situation explained above for the beam of FIGURE VI(c). The stresses presented in Appendix B for these lower sections will thus correspond to the principal stresses.

The photoelastic analysis of upper section O-M(FIGURE VI-a) showed, as expected, the presence of an isotropic region indicating the location of a neutral axis. It may be pointed out that $\tau_{xy} = 0$ along O-M. The resulting normal stress distribution along upper section O-M (σy) is shown in Appendix B.

Finally, an analysis of the frictional forces present is found in Appendix C.

All Fillet Radii (r) = 0.015"

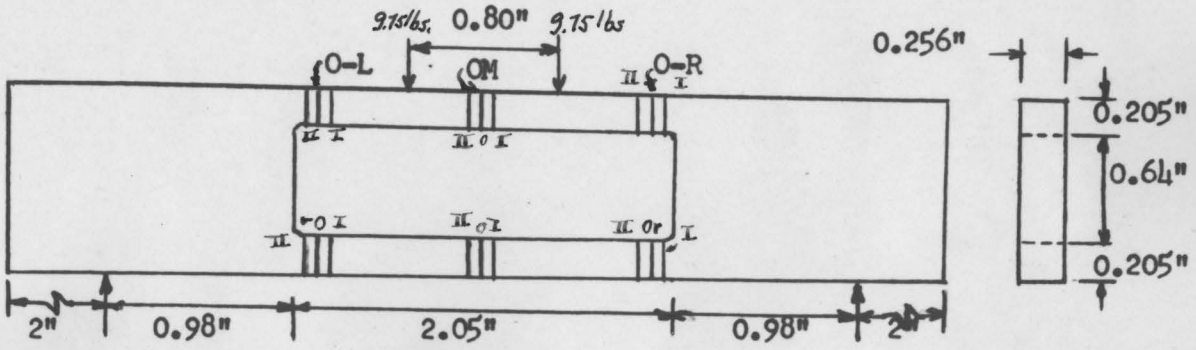

a. Dimensions of Specimen

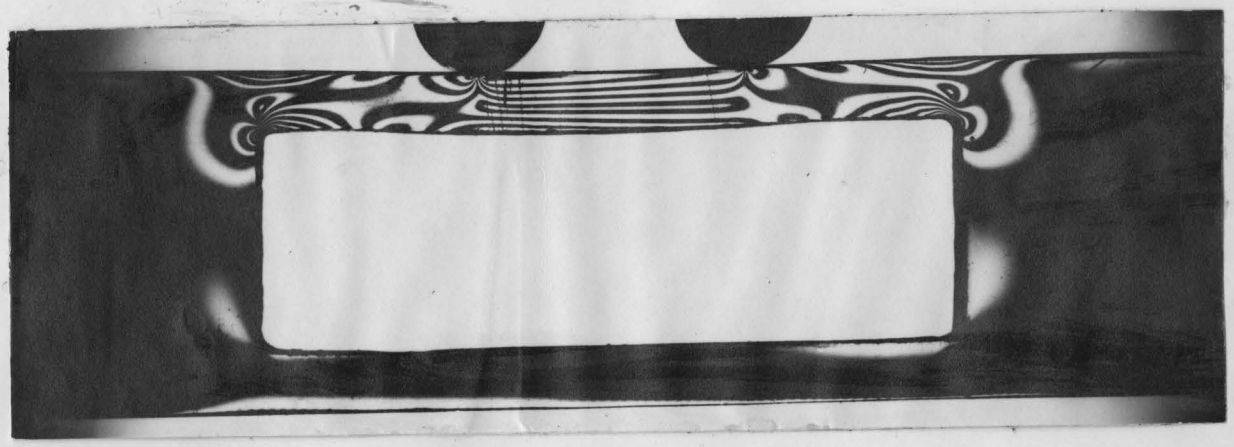

b. Problem Under Investigation

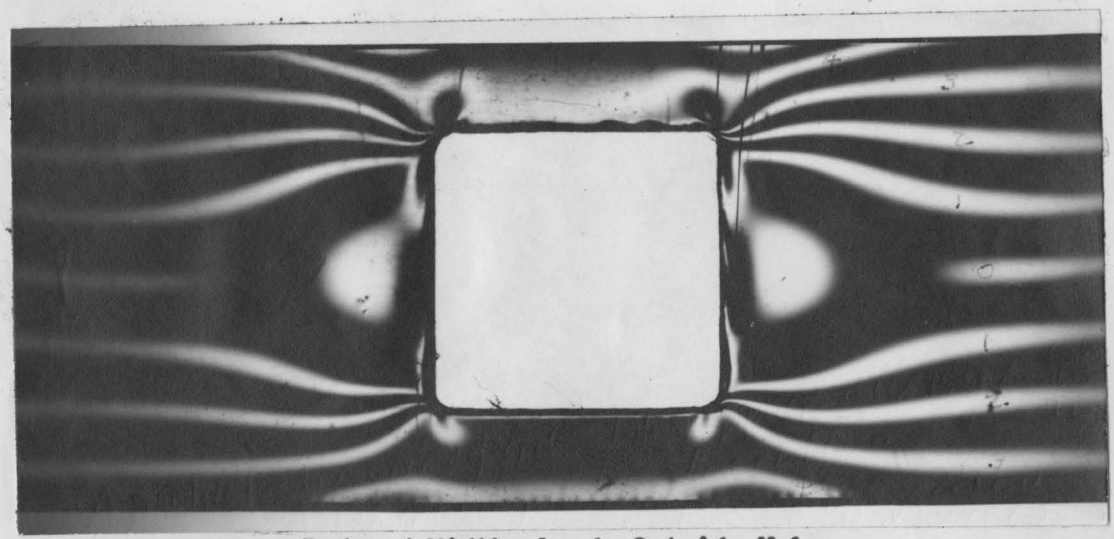

c. Reduced Width, Loads Outside Hole

FIG. VI Fringe Patterns & Dimensioned Specimen

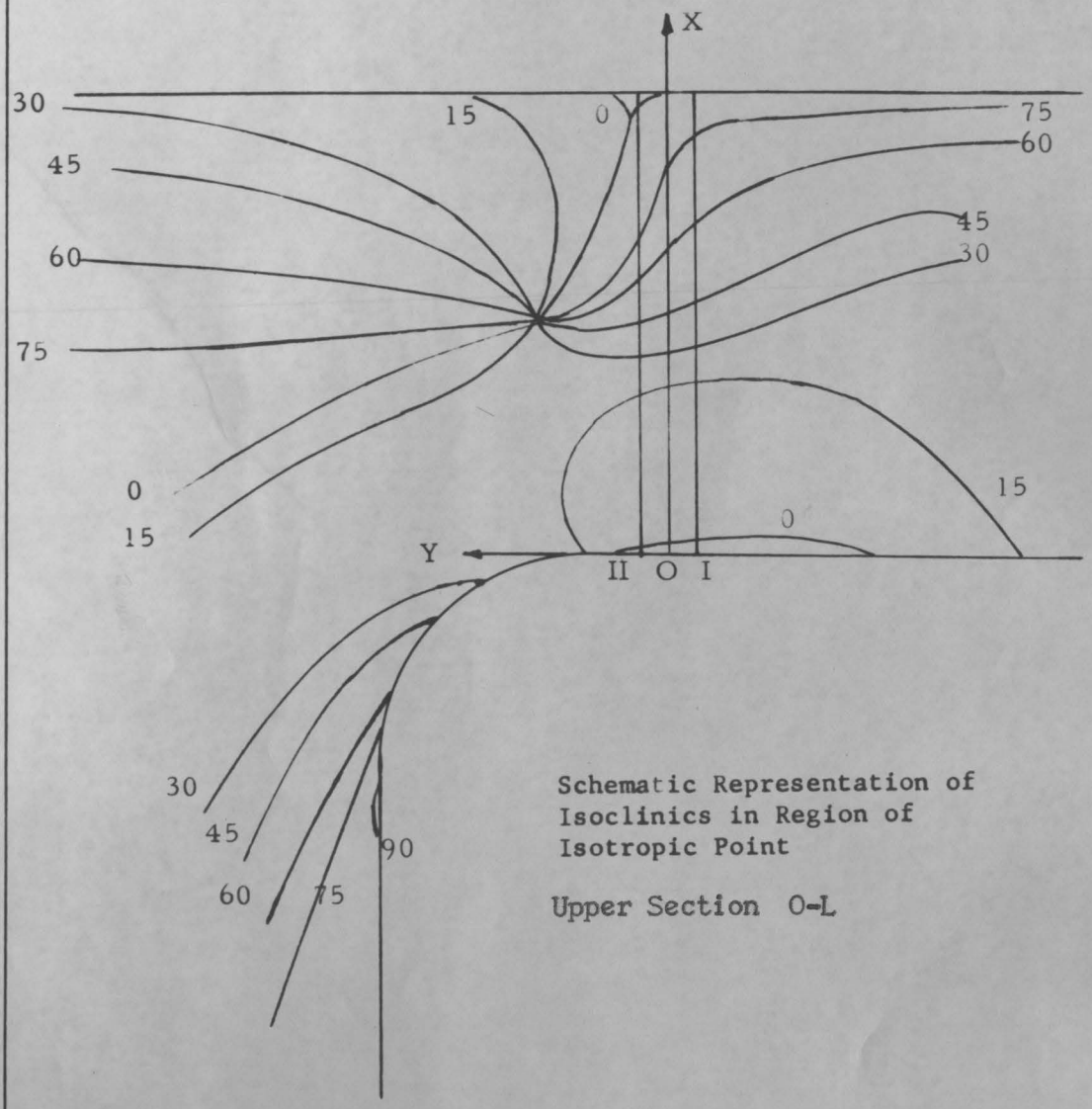

Schematic Representation of Isoclinics in Region of Isotropic Point

Upper Section O-L

Fig. VII - Superimposed Isoclinics

VIII. CONCLUSIONS

The following conclusions may be reached regarding the foregoing investigation:

a. A satisfactory method for obtaining stress-free models was developed.

b. Haloway Oil is superior to sulphuric acid for retarding time edge effects. However, machined models should not be aged in this oil.

c. Ordinary steel rollers will not eliminate frictional forces. Taped steel rollers increase these forces.

d. For the problem investigated, two reversals of curvature occurred in the section above the hole and there was some bending in the section below the hole. Also, there was no Shear in the lower portion of the beam.

IX. APPENDIX

Appendix A: The Shear Difference Method applied across Upper Section O-L as shown in FIGURE VI(a).

Abscissa scale for all curves:

1 Unit = 1/10 depth of upper section above hole = 0.0205"

Also 1 unit = distance I-II = 0.0205"

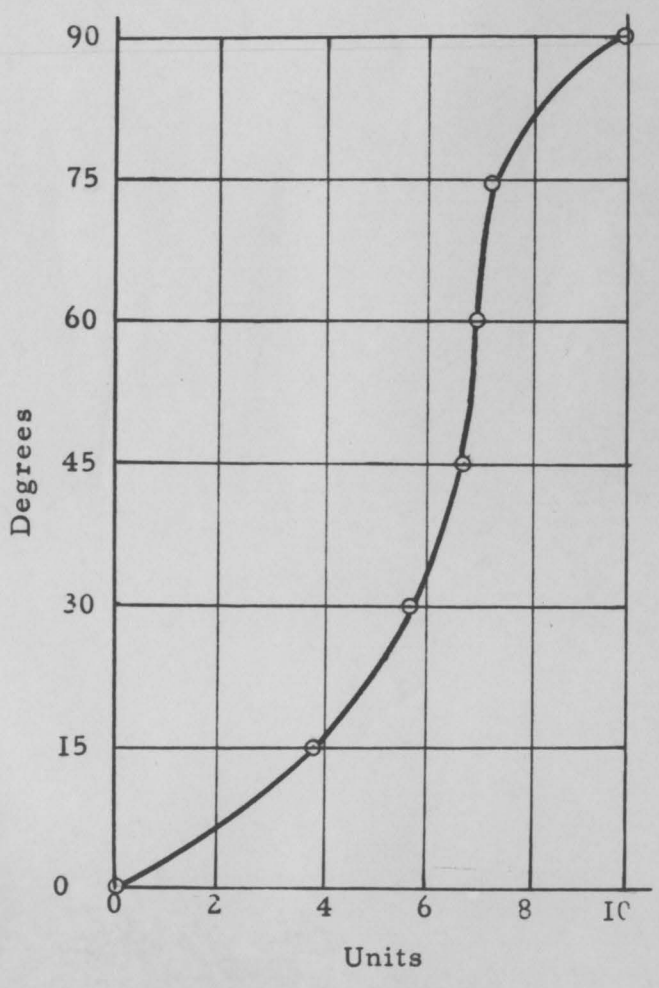

Fig. VIII
Isoclinic Parameter vs Position (Upper Portion)

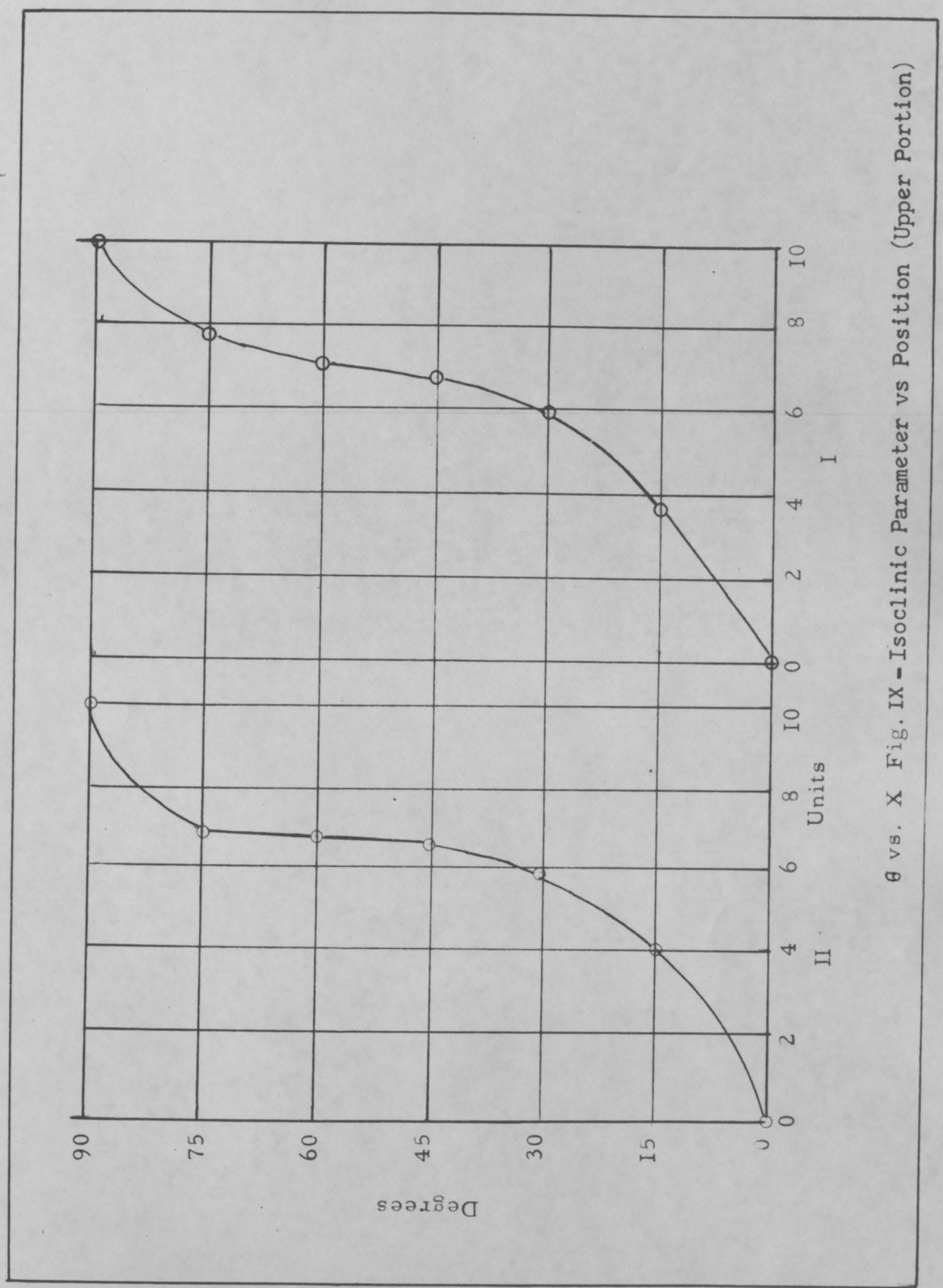

θ vs. X Fig. IX - Isoclinic Parameter vs Position (Upper Portion)

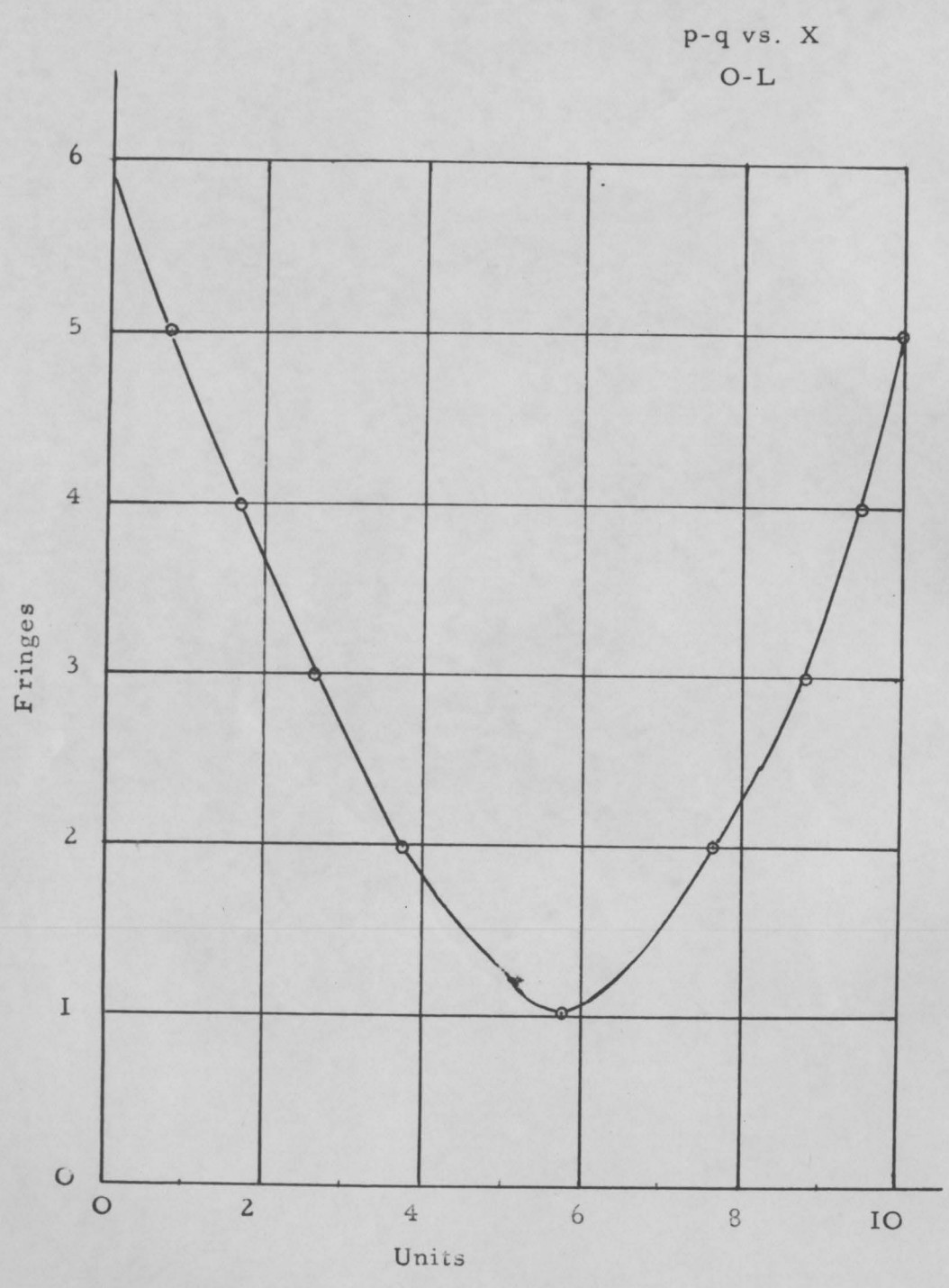

Fig. X - Upper Portion

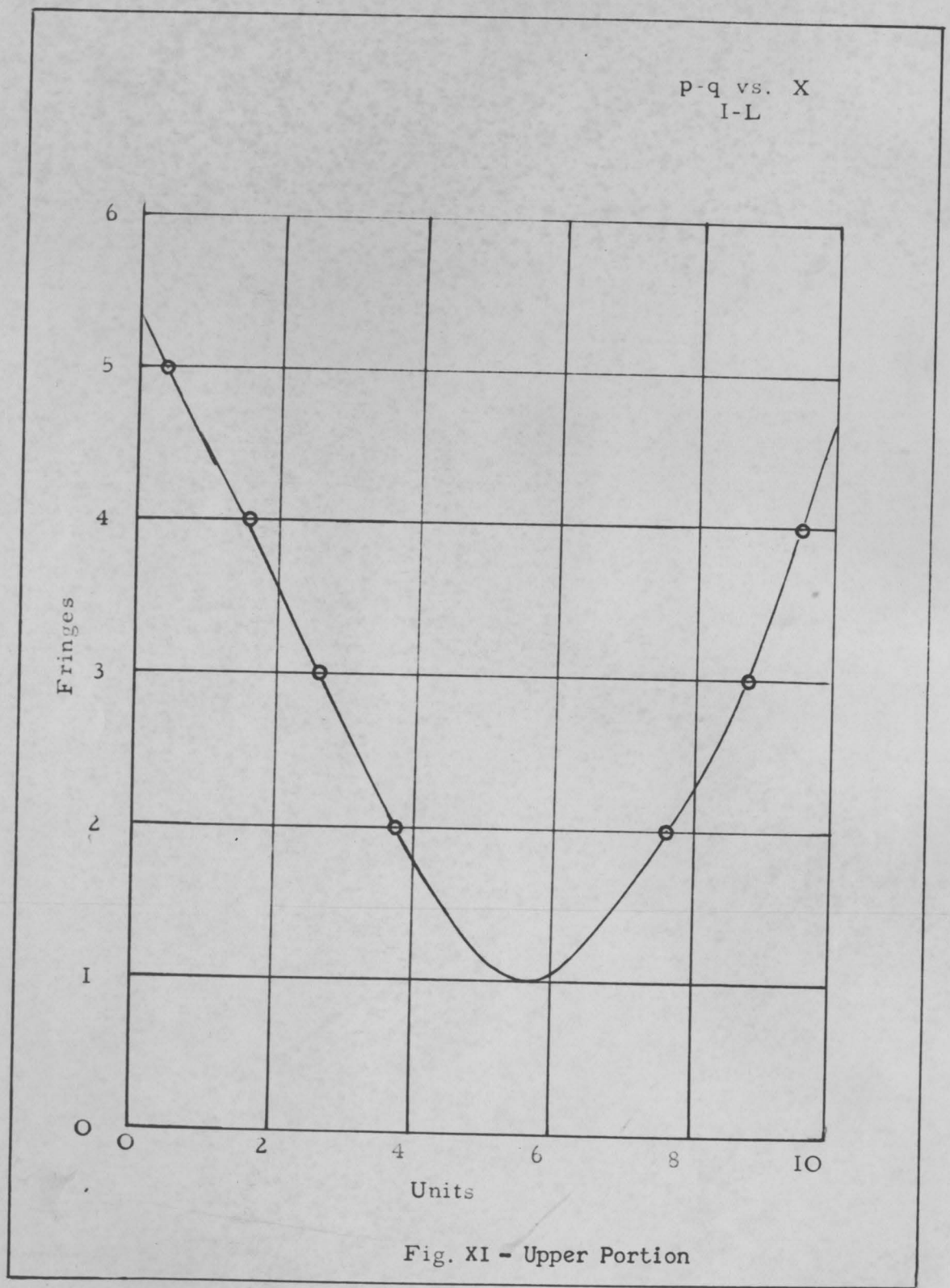

Fig. XI - Upper Portion

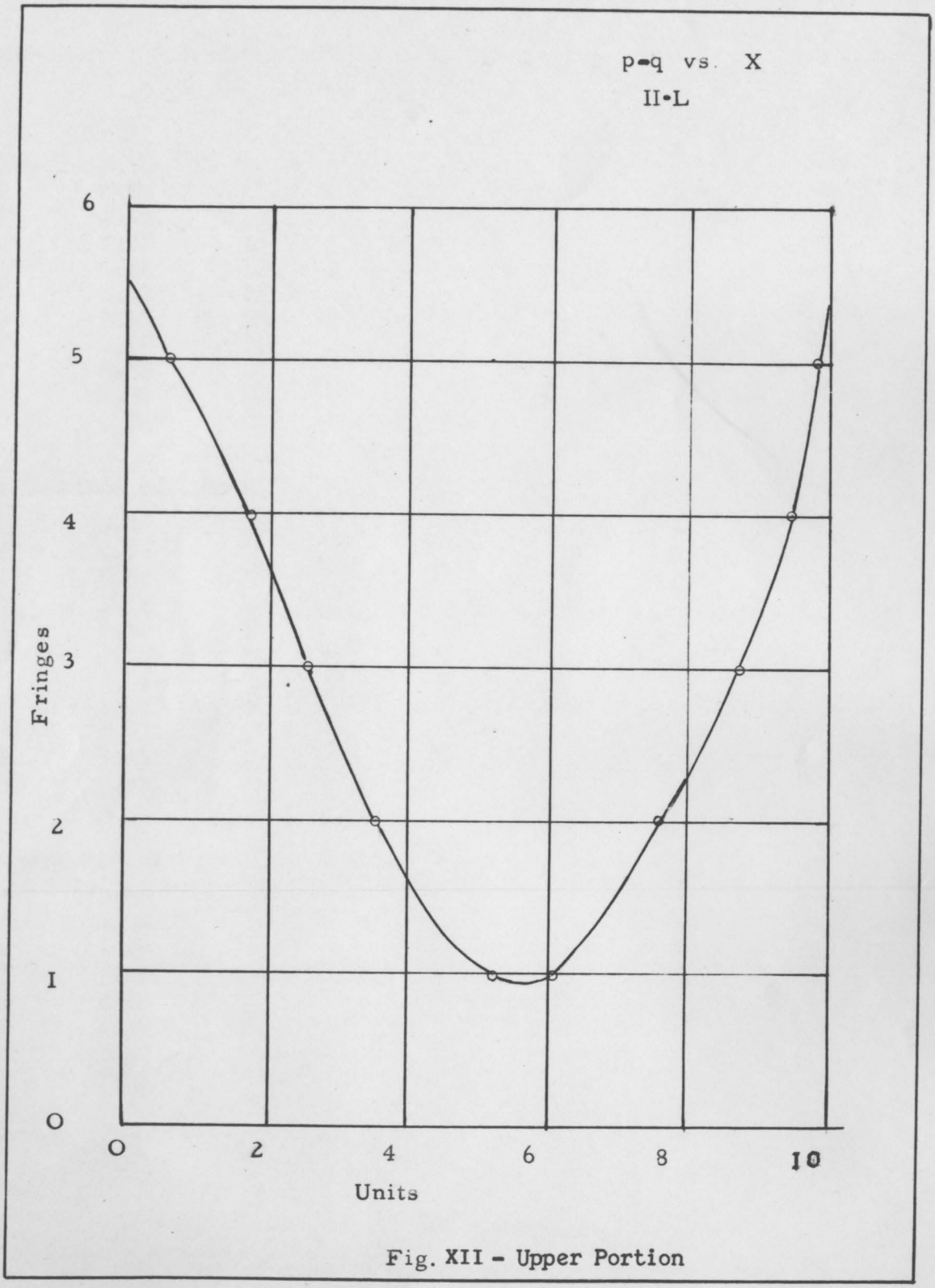

Fig. XII - Upper Portion

Computation of τ_{xy} along 0-L

Sta	p-q	θ	2θ	$180-2\theta$	sin 2θ	$2\tau_{xy}$
0	5.85	0	0	0	0	≠ 0
1	4.80	3.0	6	-	0.1045	≠0.5025
2	3.65	6.5	13	-	0.225	≠0.821
3	2.65	10.0	20	-	0.342	≠0.906
4	1.85	16.0	32	-	0.529	≠0.979
5	1.25	22.0	44	-	0.694	≠0.866
6	1.05	32.5	65	-	0.905	≠0.950
7	1.50	55.0	110	70	0.939	≠1.410
8	2.30	81.0	162	18	0.309	≠0.711
9	3.25	86.0	172.0	8	0.139	≠0.452
10	5.00	90	180	0	0	≠ 0
Computation of τ xy along II-L						
0	5.6	0	0	-	0	≠ 0
1	4.7	3	6	-	0.1045	≠0.492
2	3.80	6	12	-	0.208	≠0.79
3	2.80	10	20	-	0.342	≠0.957
4	1.70	15	30	-	0.50	≠0.850
5	1.10	21	42	-	0.668	≠0.740
6	1.00	31	62	-	0.882	≠0.88
7	1.65	49	98	82	0.989	≠1.63
8	2.35	81.5	163	17	0.292	≠0.687
9	3.45	87	174	6	0.1045	≠0.360
10	5.45	90	180	0	0	≠ 0
Computation of τ xy along I-L						
0	5.40	0	0	0	0	≠ 0
1	4.50	3.5	7	-	0.122	≠0.55
2	3.65	7.5	15	-	0.259	≠0.945
3	2.70	12.5	25	-	0.422	≠1.14
4	1.80	17.5	35	-	0.573	≠1.03
5	1.15	23.5	47	-	0.731	≠0.841
6	1.10	31.5	63	-	0.890	≠0.978
7	1.65	58.0	116	64	0.898	≠1.48
8	2.35	78.0	156	24	0.407	≠0.955
9	3.30	86.0	172	8	0.139	≠0.458
10	5.05	90	180	0	0	≠ 0

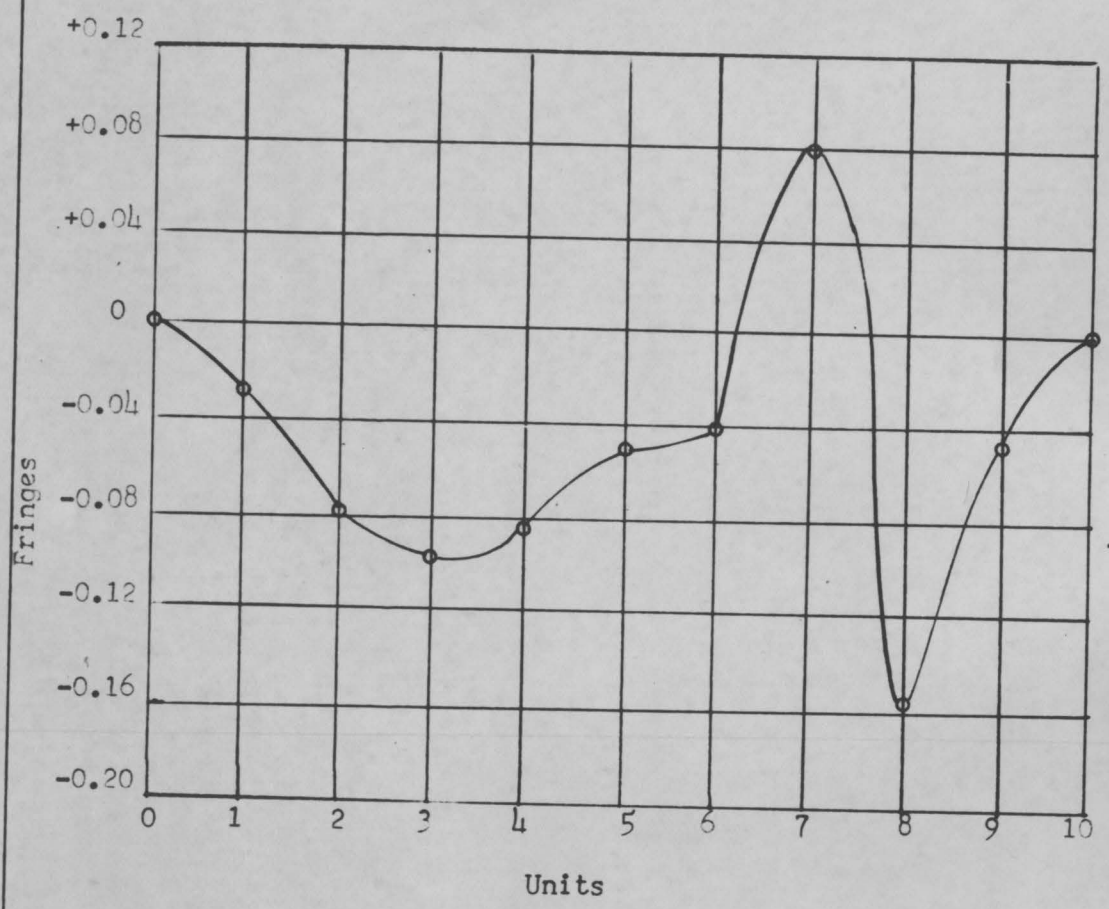

Fig. XIII - Upper Portion

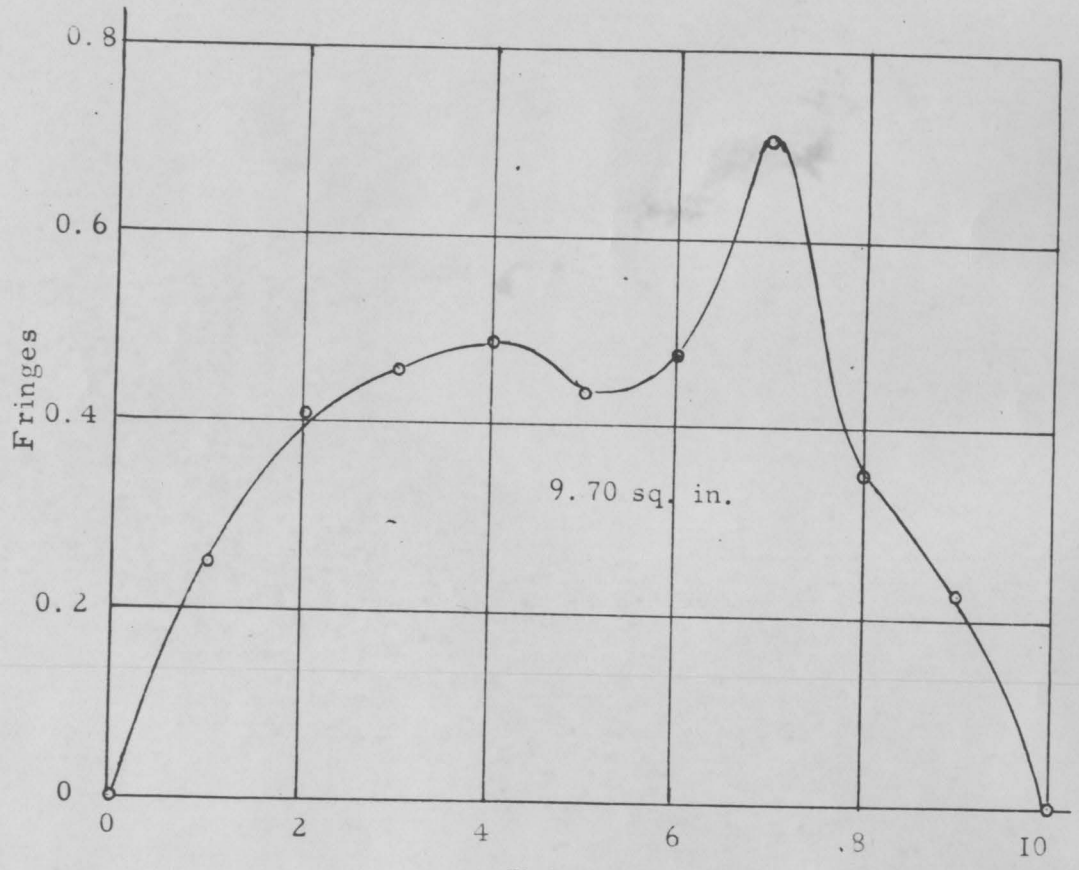

Fig. XIV - Upper Portion

Computation of σ_x, σ_y along 0-L -- Upper Sections

STA	MEAN $\Delta\tau_{xy}\frac{\Delta x}{\Delta y}$	σ_x	$\rho - q$	τ_{xy}	$\overline{\rho-q}^2$	$4\overline{\tau_{xy}}^2$	$\sqrt{\overline{\rho-q}^2 - 4\overline{\tau_{xy}}^2}$	σ_y
0		0	5.85	0	-	0	-5.85	-5.85
	-0.014							
1		≠0.014	4.80	0.25	23.1	0.252	-4.77	-4.80
	-0.054	*C-0.026						
2		≠0.068	3.65	0.41	13.3	0.673	-3.56	-3.57
	-0.088	C-0.010						
3		≠0.156	2.65	0.453	7.02	0.823	-2.49	-2.45
	-0.094	C≠0.038						
4		≠0.250	1.85	≠0.489	3.42	0.958	-1.57	-1.50
	-0.087	C≠0.074						
5		≠0.337	1.25	≠0.433	1.56	0.750	-0.82	-0.68
	-0.05	C≠0.142						
6		≠0.342	1.05	≠0.475	1.10	0.902	-0.445	-0.33
	0.0	C≠0.11						
7		≠0.342	1.50	≠0.705	2.25	1.98	≠0.519	≠0.59
	-0.05	C≠0.072						
8		≠0.347	2.30	≠0.352	5.28	0.492	≠2.18	≠2.21
	-0.012	C≠0.034						
9		≠0.359	3.25	≠0.226	10.55	0.204	≠3.21	≠3.22
	-0.024	C≠0.012						
10		≠0.383	5.00	0	-	0	≠5.0	≠5.0
		C 0						

* - c - Corrected values of σ_x based upon known boundary conditions. See FIGURE XV.

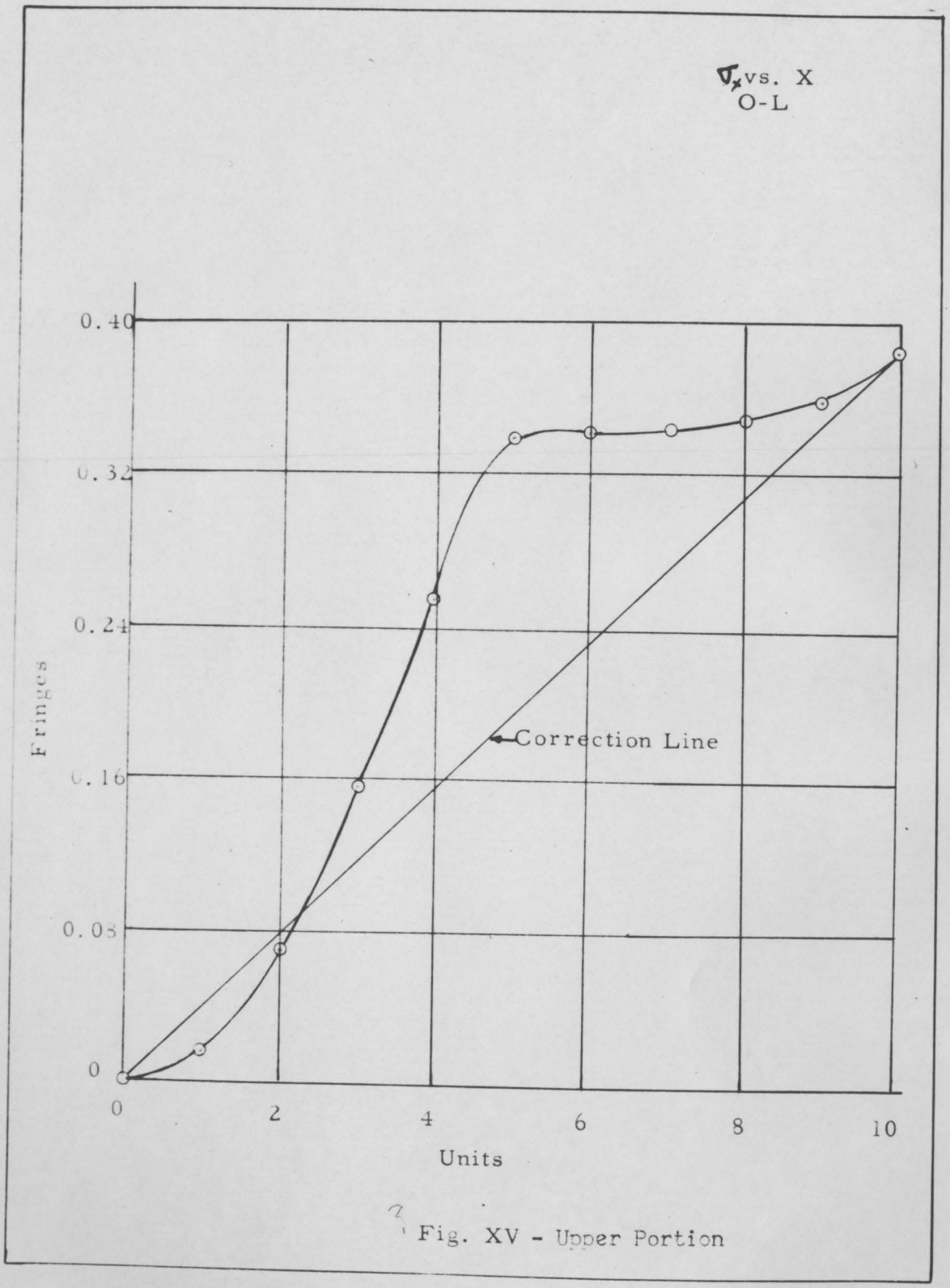

Fig. XV - Upper Portion

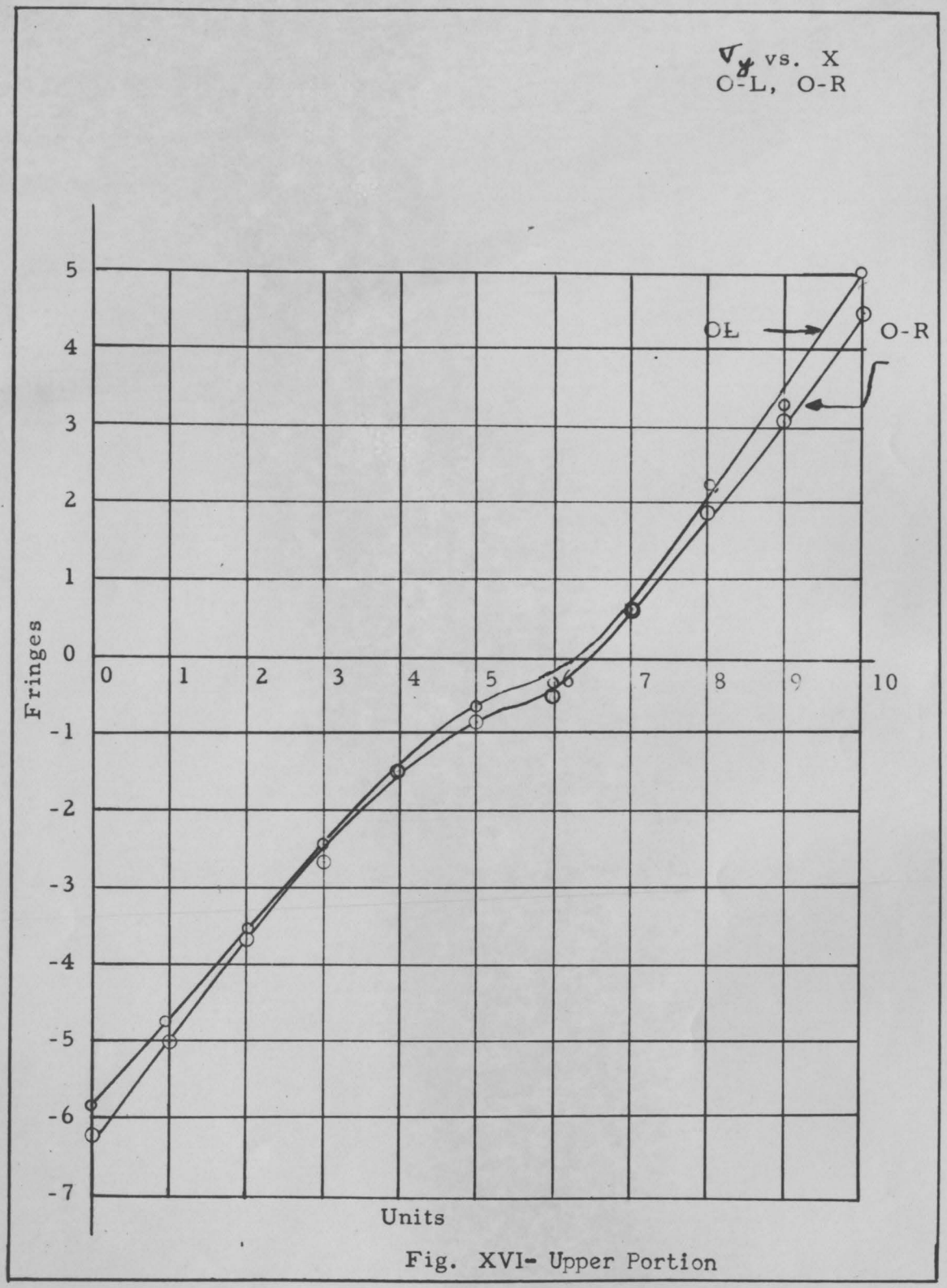

Fig. XVI- Upper Portion

Appendix B: Resulting stress distributions (σ_y) across lower sections O-L, O-M and O-R (see FIGURE VI-a) and across upper section O-M.

Scale for all abscissae:

1 unit = 1/10 depth of upper (or lower) section = .0205"

Stress distributions for sections O-L and O-R indicate dissymmetry in loading.

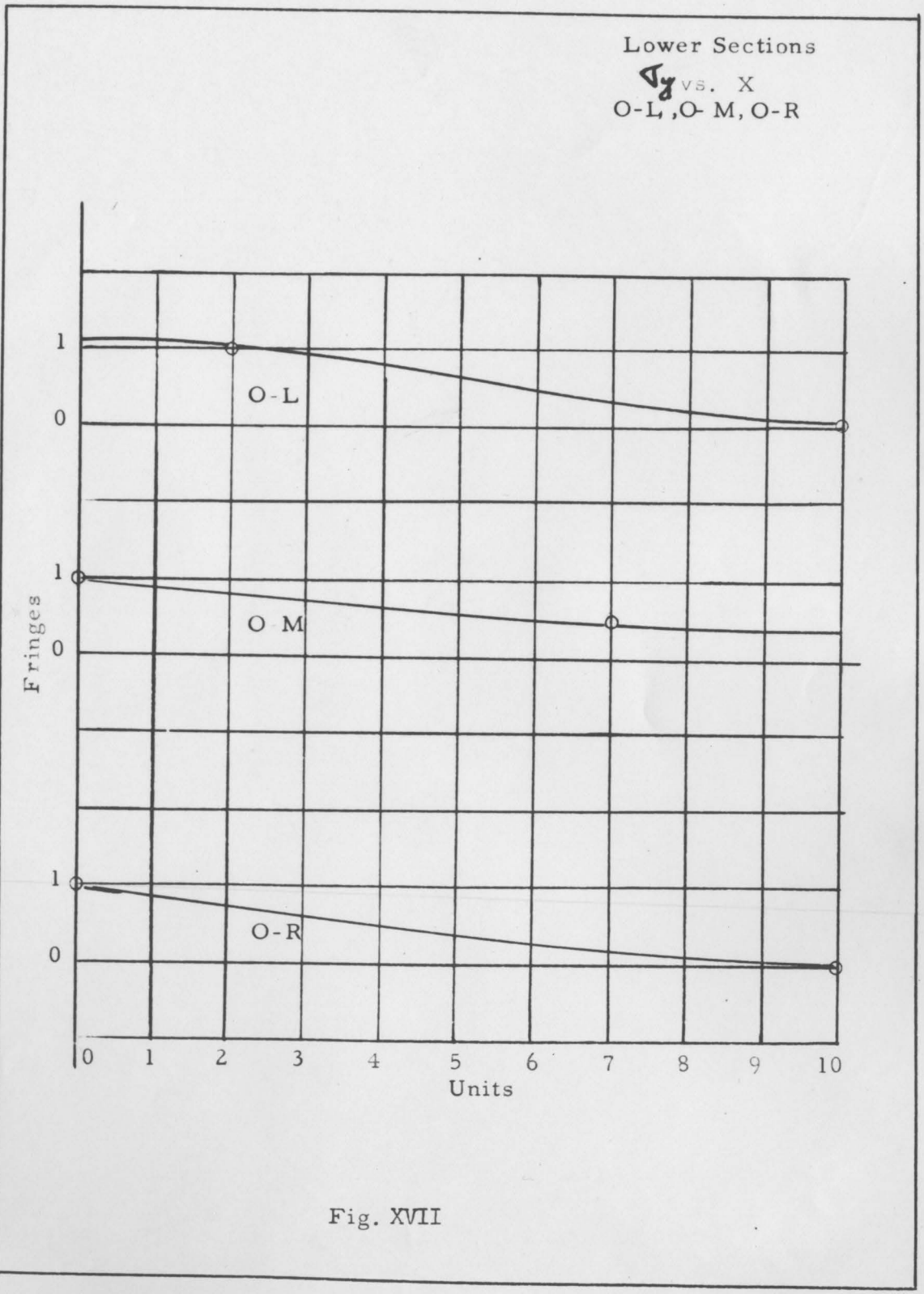
Lower Sections
∇_y vs. X
O-L, O- M, O-R
1
0
O-L
1
0
O M
1
0
O-R
Fringes
0 1 2 3 4 5 6 7 8 9 10
Units

Fig. XVII

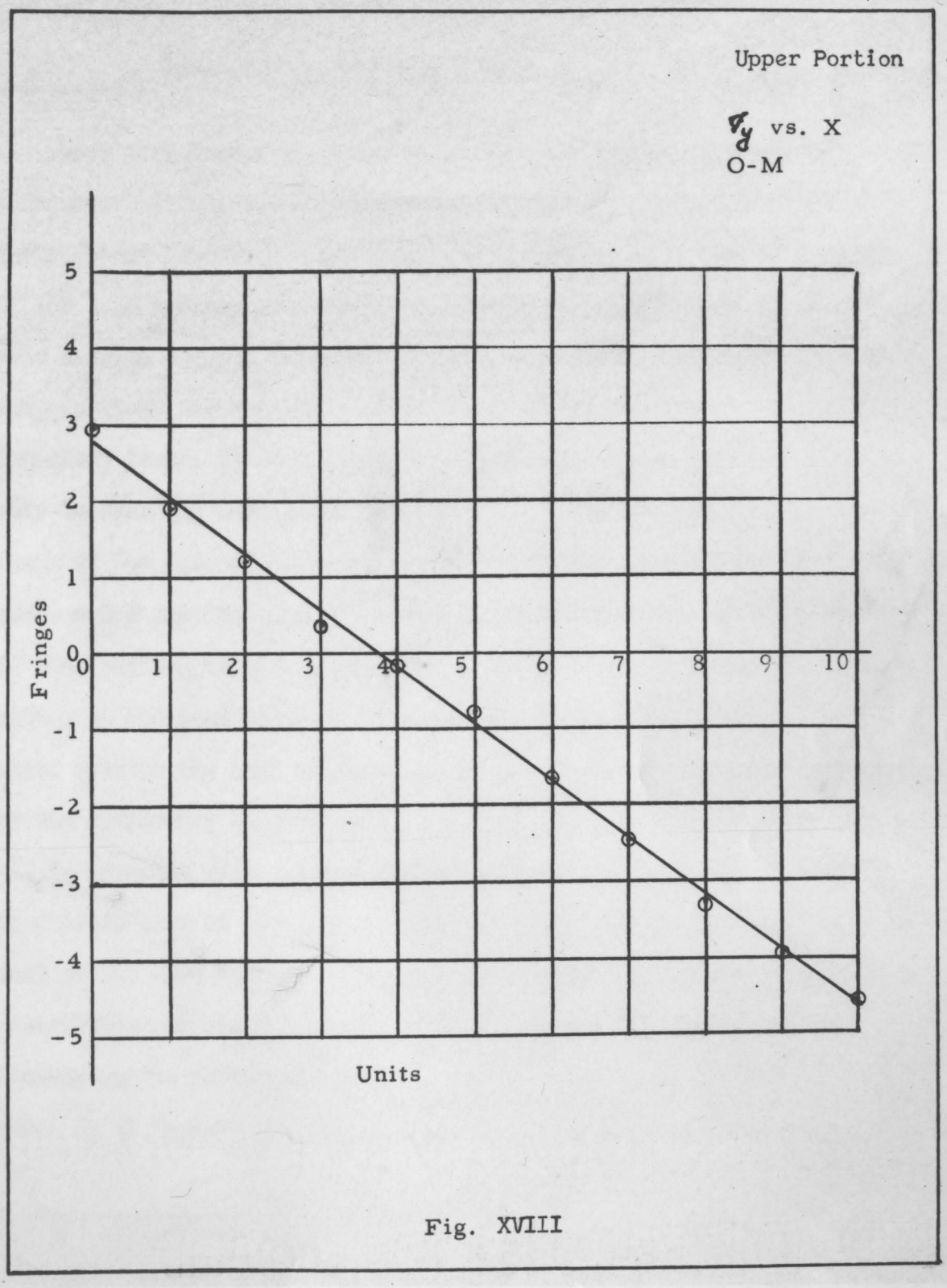
Upper Portion
σ_y vs. X
O-M
Fringes
Units
5
4
3
2
1
0
-1
-2
-3
-4
-5
0
1
2
3
4
5
6
7
8
9
10

Fig. XVIII

Appendix C: Effects of Friction Forces

When pure bending is produced through normal pin loadings on a specimen, frictional forces of considerable magnitude may result. These forces distort the stress patterns locally in the neighborhood of the load points, and they tend to decrease the value of the positive bending moment. This latter case is particularly significant where a known value of the applied bending moment is desired. In the foregoing tests, the true value of the bending moment would be of use only in checking the accuracy of the Shear Difference Method by means of the laws of statics. Since the distribution of σ_y across section O-M provides a good indication of the accuracy of the results in that region, no effort was made to reduce the frictional forces acting at the load points. Instead, the frictional forces were calculated by using the laws of statics. These forces differ mainly because of the difference in contact surface;*-at the upper portion a steel pin to specimen contact, and at the lower surface a steel pin wrapped in plastic tape to specimen contact was used. The purpose of this part of the test was to attempt to find a method for insuring a uniform distribution of the load over the thickness of the specimen without increasing the frictional forces. Upon inspection of the results in Table A, it appears that the results were strongly negative.

---

* - See also footnote on Page 39.

(Appendix C - continued)

All frictional forces, however, were considerably less than the normal loads and consequently were not considered as having important effects on the stress distribution examined. It may be noted that the upper left frictional force (Table A, Page 39) is less than half of that at upper right. Such a variation has a small effect, however, upon dissymmetry, as is evidenced by FIGURE XVI.

It should be noted that, in order to minimize the aforementioned frictional forces, a system of tension-links, as described by Frocht (1), should be employed in place of the pin loading system in FIGURE II.

Computation of Frictional Forces

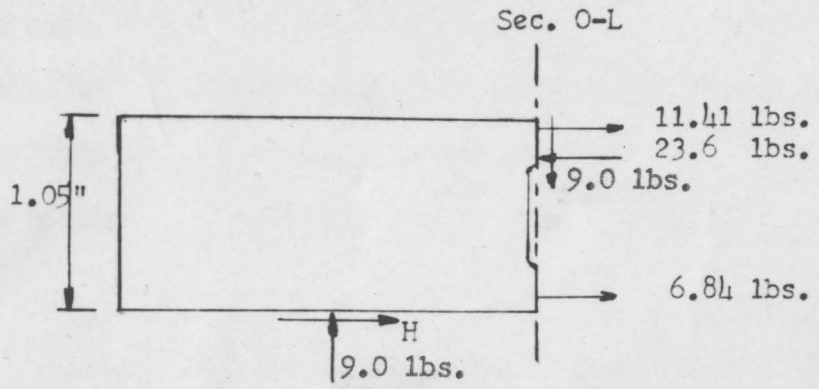

$\Sigma Fx=0 = H + 6.84 + 11.41 - 23.6 = 0$

$H = 5.35$ lbs.

% error between measured 9.75 lbs. and calculated 9.0 lbs. represents experimental error. $= \frac{0.75}{9.75} \times 100 = 7.7\%$

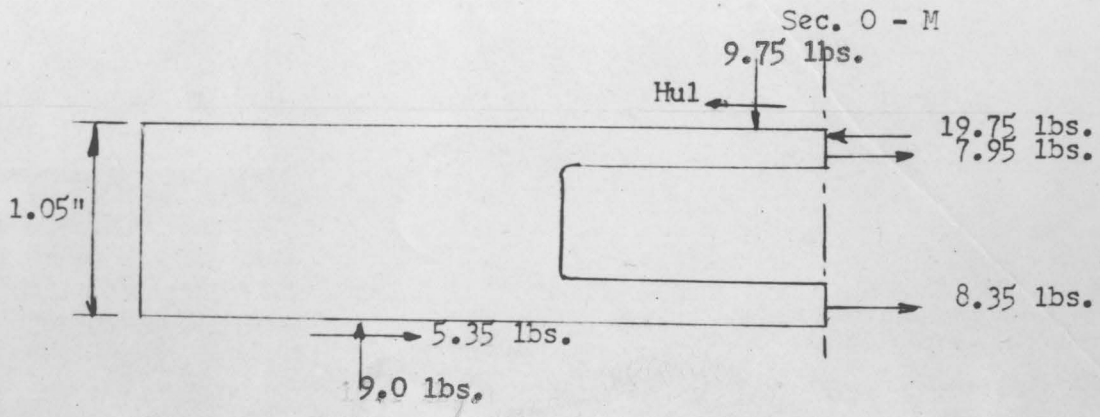

$\Sigma Fx = 0 = -Hul + 5.35 + 7.95 + 8.35 - 19.75 = 0$

$Hul = 1.90$ lbs.

Calculations for right half frictional forces would be similar to the above.

TABLE A*

Position	Contact Surface	Frictional Force
Upper Left	Steel to Specimen	1.90 lbs.
Lower Left	Taped Steel to Specimen	5.35 lbs.
Upper Right	Steel to Specimen	3.74 lbs.
Lower Right	Taped Steel to Specimen	7.27 lbs.

* In general for identical contact surfaces the lower frictional forces are somewhat smaller than the upper forces. Therefore, the values in the table should be considered qualitative rather than quantitative values. It should be noted that the differences in the frictional forces may be attributed to the dissymmetry in loading, in part, as well as differences in contact surface materials.

X. ACKNOWLEDGEMENT

The author is deeply indebted to Prof. C.W. Smith for his continued interest and guidance during this investigation.

The author also wishes to express his heartfelt gratitude and appreciation to Prof. D.H. Pletta for giving him the opportunity to undertake this investigation; also to Prof. H. Sword who assisted with some of the photography; and to Mr. G. McCauley for his skillful and untiring assistance in making the models and photographs.

XI. BIBLIOGRAPHY

1. Photoelasticity by M.M. Frocht, Vol. 1, pages 380-381.

2. Handbook of Experimental Stress Analysis by Hetenyi, pages 829-833.

3. Photoelasticity by Coker and Filon, pages 473-480.

4. Transactions of American Society of Mechanical Engineers, Vol. 56, 1934, pages 617-625. "Stress Concentration Produced by Holes and Notches" -- A.M. Wahl and R. Beeuwkes.

5. Transactions of American Society of Mechanical Engineers, Vol. 57, 1935, pages A67-69. "Factors of Stress Concentration Photoelastically Determined" -- M.M. Frocht.

6. Proceedings for the Society of Experimental Stress Analysis, Vol. IX, No. 1, pages 53-62. "Factors of Stress Concentration for the Bending Case of Fillets in Flat Bars and Shafts with Central Enlarged Section" -- Hartman and Leven.

The vita has been removed from the scanned document

ABSTRACT OF THESIS

A PHOTOELASTIC ANALYSIS OF A BEAM WITH A LARGE SYMMETRICALLY LOCATED HOLE

The particular problem, although simple in appearance from a theoretical photoelastic standpoint, involves difficult laboratory techniques.

A great deal of time and effort was spent in the preparation of a suitable model. This work was directed toward minimizing the effect of edge stresses caused by machining the material. Once a suitable model was obtained, the stress distributions across arbitrary sections were determined by use of the Shear Difference Method. Finally, results indicated the presence of frictional forces under the load and reaction points. Therefore, these forces were evaluated.